THE JOURNAL OF PHYSICAL CHEMISTRY C

Article

Cite This: J. Phys. Chem. C 2020, 124, 2420−2426

pubs.acs.org/JPCC

Defining Multiple Configurations of Rubrene on a Ag(100) Surface with 5 Å Spatial Resolution via Ultrahigh Vacuum Tip-Enhanced Raman Spectroscopy

Published as part of The Journal of Physical Chemistry virtual special issue "Toward Chemistry in Real Space and Real Time".

Jeremy F. Schultz,[†] Linfei Li,[†] Sayantan Mahapatra,[†] Chasen Shaw,[‡] Xu Zhang,[‡] and Nan Jiang*[,†]

[†]Department of Chemistry, University of Illinois at Chicago, Chicago, Illinois 60607, United States

[‡]Department of Physics and Astronomy, California State University, Northridge, Northridge, California 91330-8268, United States

Supporting Information

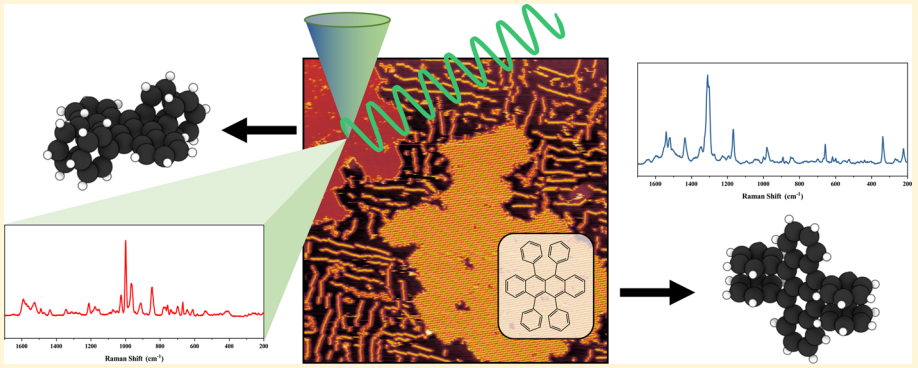

ABSTRACT: Flexible polycyclic aromatic hydrocarbons (PAHs) have experienced a surge of research with the discovery of nanographenes that can be fabricated on surfaces. The flexibility in σ bonds within aromatic compounds is carefully managed in order to induce particular binding configurations on a surface that are capable of undergoing cyclodehydrogenation reactions or exhibit unique material functionalities. The structure of adsorbed organic molecules is essential to the design of thin films of these compounds. Highly localized chemical effects must be considered due to sensitivity to defects or amorphous character that destroys the useful properties of the film. Here, ultrahigh vacuum (UHV) scanning tunneling microscopy (STM) and tip-enhanced Raman spectroscopy (TERS) have been used to characterize the self-assembly of rubrene on Ag(100). Through comparison with time-dependent density functional theory simulations, the configuration and orientation of rubrene molecules on the surface are defined with ångström scale resolution.

INTRODUCTION

Thin films of organic molecules on surfaces offer the means to develop new devices with exotic properties via the self-assembly of molecules on surfaces.[1] Crucially, these methods depend upon an understanding of the mechanisms and forces that drive the formation of supramolecular structures.[2] In the case of soft organic compounds, flexibility of the molecular entities complicates the viability of the system and the growth of self-assembled layers.[3] This is especially true in the case of rubrene (5,6,11,12-tetraphenyltetracene), where the charge carrier properties of semiconductor single crystals of rubrene depend upon the degree of molecular order. Rubrene is the organic semiconductor with the highest carrier mobility, but this only occurs when the molecules are highly organized and adopt planar configurations in the crystal phase.[4] As a result, identification and characterization of the configurations of organic molecules on a surface are critical to the design of these devices.

Scanning tunneling microscopy (STM) combined with tip-enhanced Raman spectroscopy (TERS) has been proven as an analytical technique to fully characterize molecular systems at interfaces with spatial resolution at the subnanoscale.[5−8] When flexible molecules can adopt different configurations even within one self-assembly, spectroscopic characterization of each individual species requires ångström scale resolution. The plasmonic tip enhancement of TERS results in a highly localized field that strongly enhances the near field signal, allowing systems to be probed spectroscopically well below the

Received: September 27, 2019
Revised: November 1, 2019
Published: November 4, 2019

DOI: 10.1021/acs.jpcc.9b09162
J. Phys. Chem. C 2020, 124, 2420−2426

diffraction limit.[9−12] This spatial resolution combined with the sensitivity of Raman spectroscopy to intermolecular interactions and binding configurations can be used to effectively and uniquely characterize the self-assembly of organic molecules on surfaces.[13−16] Here, we demonstrate TERS fingerprints for a two-dimensional phase segregation between two adjacent binding configurations of rubrene molecules with 5 Å resolution. Through comparisons of TERS fingerprints with simulated spectra, which were built with consideration for the flexibility in the molecular structure, the orientation of molecules can be defined.[17−21]

Rubrene is a red colored polycyclic aromatic hydrocarbon commonly used in organic light-emitting diodes (OLEDs) and organic field-effect transistors.[22] These applications depend critically upon the ability to grow well-ordered crystalline thin films.[23] Previous studies of rubrene thin films have found a tendency toward amorphous structures, which has been attributed to its ability to adopt multiple orientations.[22−24] In this study, we have applied ultrahigh vacuum (UHV) STM-TERS to the study of rubrene on a Ag(100) substrate, revealing four stable binding configurations and characterizing the molecule−molecule and molecule−substrate interactions that determine its self-assembly with spatial resolution that allows the discrimination of individual adjacent molecules.

EXPERIMENTAL AND THEORETICAL METHODS

Experiments took place in a variable temperature STM system (Unisoku) under ultrahigh vacuum at a base pressure of 8.0×10^{-11} Torr. The Ag(100) single crystal (Princeton Scientific, 99.999% purity) was prepared in a preparation chamber with a base pressure of 1.0×10^{-10} Torr. The Ag(100) substrate was cleaned by cycles of argon sputtering and indirect thermal annealing to 800 K. The rubrene molecules were purchased from Sigma-Aldrich (sublimed grade, 99.99%) and deposited via a K-cell style molecular evaporator (175 °C) to obtain submonolayer coverage. The sample was at room temperature during deposition. The sample was then transferred to the STM chamber for STM imaging and TERS experiments. These experiments all took place at liquid nitrogen temperatures (78 K). The STM was operated in constant current mode with the bias applied to the sample with respect to the grounded tip. Electrochemically etched Ag tips were used for STM imaging and TERS experiments. Gwyddion was used for STM image processing.[25]

A 515 nm solid-state CW laser (Cobolt) polarized parallel to the Ag tip was used as the excitation source for TERS experiments. The optical setup has been described in detail previously.[17] Significantly, the STM chamber is equipped with in-vacuo lenses positioned in close proximity to the tip to allow for optimal laser spot focusing and collection efficiency. All spectra shown have a 3 s acquisition time to minimize thermal drift in spatial mapping experiments, while the incident laser power was 500 μW.

In our density functional theory (DFT) simulations, we used a four-layer slab with a (5×5) unit cell for the Ag(100) surface. The atoms in the top two layers were fully relaxed while the rest of the atoms were fixed in their equilibrium positions. The adsorption energy of a rubrene molecule on the Ag(100) surface was determined by

$$E_{ads} = E_{[Ag100+rubrene]} - E_{[Ag100]} - E_{[rubrene]}$$

where $E_{[Ag100+rubrene]}$ and $E_{[Ag100]}$ are the total energies of the Ag(100) surface with and without the rubrene adsorbate, respectively. $E_{[rubrene]}$ is the total energy of a stand-alone rubrene molecule. The DFT calculations were carried out using the VASP package[26] with the projector augmented wave pseudopotentials[26,27] and the Perdew−Burke−Ernzerhof generalized gradient approximation.[28] An energy cutoff of 400 eV was used for the plane-wave basis set. Only the Γ-point was considered in the Brillouin zone due to the large size of the supercell, which had been tested to yield the converged results. The van der Waals (vdW) interaction is described by the semiempirical DFT-D2 scheme of Grimme,[29] and the C_6 coefficients of C, H, and Ag are chosen to be 1.75, 0.14, and 81.24 J × nm^6/mol, respectively. The force convergence criterion for atomic relaxation is 0.01 eV/Å.

The Raman spectrum, separated into Cartesian coordinates α, was determined by the derivatives of the polarizability tensors $\tilde{\alpha}_{\alpha\alpha}(\omega)$ with respect to the Ith mass-weighted normal mode Q_I, which is computed on the basis of the double harmonic approximation:

$$\frac{d\tilde{\alpha}_{\alpha\alpha}(\omega)}{dQ_I} = \sum_{\xi} \frac{d\tilde{\alpha}_{\alpha\alpha}(\omega)}{d\xi} E_{I,\xi}$$

where ω is the frequency of incident light, ξ is the atomic coordinate, and $E_{I,\xi}$ is the eigenvector of the Ith phonon mode. The vibrational eigenmodes of the adsorbed rubrene were obtained in the presence of the Ag surface by solving the eigenvalue problems of a dynamical or Hessian matrix based on density functional perturbation theory (DFPT) calculations.[30] The effect of the Ag substrate on the molecular vibration was thus captured. We found that the adsorption of rubrene on the Ag(100) is physisorption due to the vdW interaction and thus the effect of the Ag surface on the electronic structure of rubrene is negligible. Therefore, the polarizabilities of rubrene can be computed without the presence of the Ag substrate. The derivatives of polarizability, $d\tilde{\alpha}_{\alpha\alpha}(\omega)/d\xi$, of the rubrene under its adsorbed configuration were then calculated by employing our recently developed time-dependent density functional theory (TDDFT) approach.[31] The frequency ω was chosen to be close to the most red adsorption peak of rubrene at 526 nm which is consistent with experiments.[32−34]

RESULTS AND DISCUSSION

Scanning Tunneling Microscopy. The self-assembly that results from the deposition of rubrene onto a Ag(100) substrate at room temperature was visualized via STM imaging. Previous research by Pivetta et al. found that rubrene on Ag(100) forms close-packed arrangements, with coverage dependent supramolecular assemblies observed on other surfaces.[35] Our STM results show similar close-packed self-assembled islands, but in contrast we observed diversity in the self-assembled structures formed on Ag(100). As seen in Figure 1, there is evidence for two different types of molecular islands as well as molecular chains.

The structure of rubrene is well-known to exhibit flexibility, with two distinct and very different conformations possible depending on its local chemical environment. The tetracene backbone can be twisted (fully relaxed) or planar (constrained), with DFT calculations predicting that the twisted conformation is more favorable for an isolated molecule.[23] Current interpretations of the configurations of rubrene on surfaces rely upon STM to observe supramolecular assemblies[36,37] or surface spectroscopic techniques, such as near edge

DOI: 10.1021/acs.jpcc.9b09162
J. Phys. Chem. C 2020, 124, 2420−2426

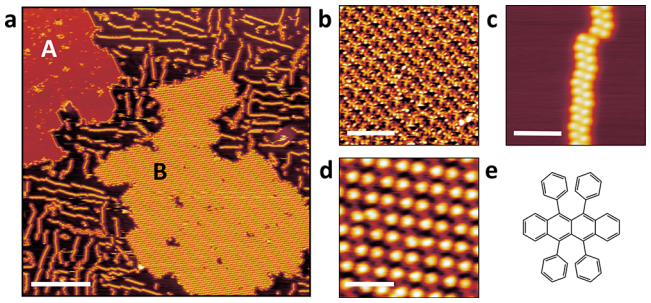

Figure 1. (a) Zoomed-out STM image of the self-assembly of rubrene on the Ag(100) substrate where the three different types of self-assembly are visible. Scale bar represents 50 nm. (b) Zoomed-in STM image of the dimmer A island, where intramolecular resolution is evident. (c) Zoomed-in STM image of the dimeric chain assembly (U = +1 V, I = 100 pA). (d) Zoomed-in STM image of the brighter B island. (e) Chemical structure of the rubrene model with tetracene backbone and substituent phenyl groups. Conditions for all of the STM images were U = +1 V, I = 100 pA. In the case of zoomed-in images the scale bar designates 5 nm.

X-ray absorption fine structure[38] and ultraviolet photoelectron spectroscopy.[39,40] In some cases, these spectroscopic techniques have revealed the presence of multiple configurations of rubrene present on the surface. However, although these techniques reveal these possibilities, a spatially resolved understanding of the multiple configurations that can occur on the surface remains elusive through these ensemble-based measurements.

On the contrary, STM experiments can prove the presence of different configurations of molecules with supreme spatial resolution.[39,41] The self-assembly of rubrene on various surfaces can result in complexity in the form of chiral supramolecular aggregates[36,42,43] or it can form molecular islands[24,35] depending upon the substrate. In the case of this experiment, three different unique self-assemblies of rubrene were observed to form on the Ag(100) surface with submonolayer coverage. Figure 1b depicts a zoomed-in image of the dimmer island visible in Figure 1a. This type of molecular island will be referred to as island A. In a similar manner, Figure 1d depicts the brighter island that appears in the adjacent large-scale STM image, which will be referred to as island B. Finally, Figure 1c presents the chain-like structure that appears to spread across the substrate surface. Significantly, over the course of scanning multiple days and repeat preparations of this sample, these multiple assemblies were found to occur in similar proportions, suggesting similar stabilities on the surface.

STM experiments were used to offer a preliminary interpretation of molecule−molecule and molecule−substrate interactions. In the A island, intramolecular features are visible, in agreement with previous studies of rubrene on Ag surfaces.[37] Through comparison with the chemical structure, shown in Figure 1e, it becomes possible to define a tentative understanding of the interactions and binding configurations that define this self-assembly. The tetracene backbone and four phenyl groups appear to be visible in the STM imaging. The apparent length of the tetracene backbone suggests it lies parallel and primarily planar to the surface. Meanwhile, the phenyl groups appear narrow with orientations more perpendicular to the substrate. The A island is the most densely packed and this fact taken in consideration with the apparent molecular conformations leads to the conclusion that $\pi-\pi$ and $\pi-$H interactions are the driving forces to form this ordered island.[44]

Although STM is an extremely powerful spatially resolved surface science technique, it is not ideally suited for all chemical systems. SPM techniques, such as STM and noncontact atomic force microscopy (nc-AFM), excel at visualizing planar, larger, aromatic molecules. With functionalized tips nc-AFM has even generated images of intramolecular bonds, resolving internal structures of molecules, as well as intermolecular bonds or interactions.[45,46] However, these experiments require flat molecules with stability that is typically only available when the sample is held at temperatures below ∼15 K. STM is complicated by the fact that all of the images are generated via a feedback loop that depends upon tunneling electrons, ultimately revealing images of the electronic structures of the molecules and substrate that arise from probing the local density of states (LDOS).[47] As a result, STM imaging can sometimes have issues with resolving the binding configuration of molecules on a surface if they are nonplanar, smaller, or other factors prohibit resolving intramolecular features.

In this experiment, STM revealed unique binding configurations of rubrene that results in the B island and chain supramolecular assemblies, but intramolecular resolution was not possible. Significantly, the chains are observed to consist of pairs of rubrene molecules perpendicular to the chain direction. And the B island appears to consist of molecules that are packed less densely than ones in A islands. The molecules in the B islands and chains appear brighter than those in the A island. However, this brightness does not necessarily correspond with topology, as it depends upon the LDOS as previously mentioned. The final conclusion made from STM imaging is that the dimmer A island is bounded by brighter molecules, perhaps implying that a lack of intermolecular interactions results in this brighter configuration. Although the spatial resolution of STM revealed the presence of multiple configurations, another technique was required to properly identify the configuration and orientation that rubrene adopts on the Ag(100) surface.

Tip-Enhanced Raman Spectroscopy. Studies of rubrene on surfaces are commonly combined with a spectroscopic technique that assists in the interpretation of the STM results. Critically, these spectroscopic methods typically have far less spatial resolution than STM, resulting in the convolution of multiple configurations in the spectra.[48] An ideal solution allows for spectra to be acquired with spatial resolution on par with STM imaging. In this experiment, we supplement our initial STM-based interpretation with TERS. As a result of the extremely localized enhanced electromagnetic field generated at the tip apex, Raman signal of a single molecule becomes possible,[9,49−51] and with certain systems, intramolecular resolution has been proven with imaging resolved at the Ångström level.[52,53] In this manner, the tandem technique of STM-TERS presents as an ideal method to characterize the multiple configurations of rubrene found in our experiment.[54]

TERS spectra revealed vibrational fingerprints for each supramolecular structure of rubrene observed with STM. Figure 2 depicts representative spectra obtained for A islands, B islands, and chains. The fingerprints for B islands and chains appear remarkably similar. Comparison of the spectra for B islands and chains also confirms the initial conclusion that rubrene molecules adopt similar configurations in B islands and chains, which was made from STM, based upon the similar

DOI: 10.1021/acs.jpcc.9b09162
J. Phys. Chem. C 2020, 124, 2420−2426

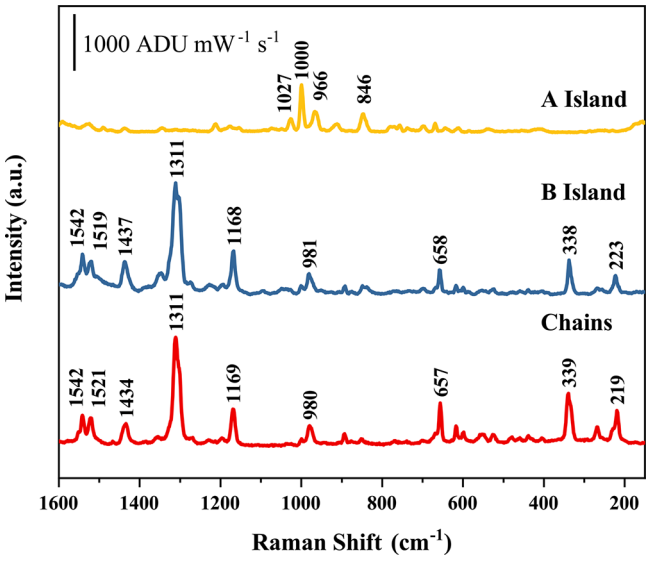

Figure 2. TERS spectra of the various assemblies of rubrene on the Ag(100) substrate. Each spectral fingerprint is labeled with the appropriate self-assembly. The TERS enhancement is denoted with the scale bar in the top left corner.

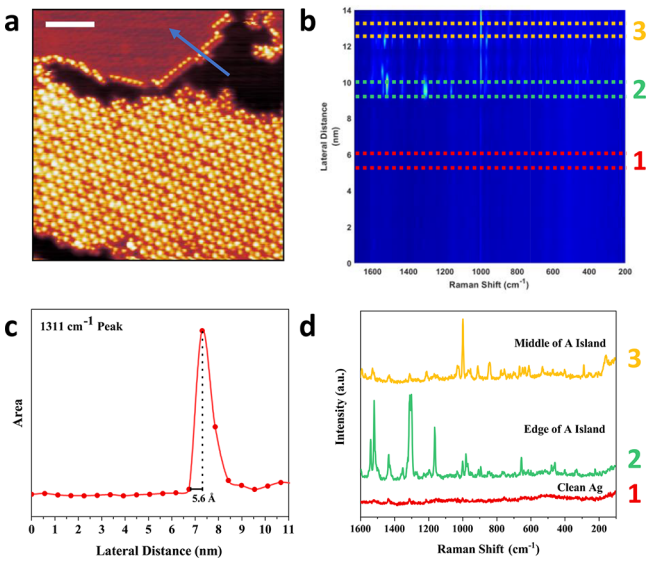

Figure 3. (a) STM image of an A island and B island adjacent to each other. The bright boundary of molecules surrounding the A island is apparent. The arrow denotes the direction and location of the TERS line profile that was acquired ranging from the bare Ag substrate to an A island. The scale bar represents 10 nm (U = +1 V, I = 100 pA). (b) Waterfall plot representing the spectra acquired for the line profile. (c) Line profile of the area of the peak at 1311 cm^{-1}. The relevant section of the line profile has been chosen to highlight the intensity at the boundary of the A island. (d) Representative spectra of the clean Ag substrate where no signal was observed, the fingerprint from the edge of the A island, and a spectrum from the middle of the A island. These are selected spectra from the line profile.

brightnesses of the rubrene molecules found in these two self-assemblies. Due to the reduced signal in the spectra for an A island, it is expected that the rubrene molecules within an A island adopt a more planar configuration with the tetracene backbone parallel to the metal surface,[55,56] which was an earlier assumption based upon STM imaging. Beyond the overall reduced intensity, the notably different spectrum for the dimmer A island corroborates the assesment that the molecules adopt a significantly different configuration in this island.

The spatial resolution of TERS allows for the identification of multiple orientations within one self-assembly. In Figure 1a there is an outline of bright molecules surrounding the dimmer A island at its boundary. Furthermore, an STM line profile across this boundary compared to a profile of molecules in a chain is presented in Figure S1. A TERS line profile permits a better understanding of the configuration of the rubrene molecules that surround the A island. The results of this experiment are represented below in Figure 3. The first part of this figure shows an STM image with both an A island and a B island. In order to characterize the brighter boundary of the A island a line of sequential spectra were acquired across the boundary from the bare Ag substrate to the dimmer molecules in the A island. The distance between points was chosen to be 5.6 Å in order to capture the fingerprint corresponding to the edge of the A island. A waterfall plot of these spectra appears in Figure 3b, with representative spectra of the different categories below in Figure 3d. Notably, the bare Ag substrate reveals no signal. Additionally, representative tip engaged and tip retracted spectra are presented in Figure S2, to confirm the tip remains clean and uncontaminated during the course of experiments. As the tip progresses over the boundary, a vibrational fingerprint is obtained that is markedly similar to the spectra obtained for B island and chains. Proceeding toward the middle of the island, this signal is immediately replaced by the A island signal that appears in Figure 2. In order to track this change, we fit the peak located at 1311 cm^{-1}, which is the most notable peak for a rubrene molecule in a B island or chain, and plotted its area against the lateral distance of the tip. This plot appears in Figure 3c. The area of this peak revealed the spatial resolution of TERS to be 5 Å, identifying different binding configurations of rubrene that are directly adjacent to each other on the surface. Additional methods of calculating the spatial resolution of TERS are included in the Supporting Information appearing in Figure S3 alongside an STM line profile showing the apparent size of a rubrene molecule at the boundary as observed with STM.

In order to fully understand the TERS fingerprints of rubrene and assign the binding configurations of the molecules on the surface, we resorted to TDDFT calculations. We first performed DFT simulations to obtain the energetically stable structures of rubrene on the Ag(100) surface based on speculated configurations. Then, we computed the spectra of these configurations, which we compared to the positions and relative intensities of vibrational modes found in the experimental spectra. Multiple expected binding configurations and orientations were used in these preliminary steps in order to find the best match between the calculated spectrum and the experimental data. The successful attempts appear in Figures 4 and 5, while other attempts are included in the Supporting Information in Figure S4. The binding configuration can thus be obtained by matching the experimental spectra. We begin with the A island assembly, where a planar configuration is expected on the basis of initial interpretations. The simulated spectrum separated into x-, y-, and z-components compared to the experimental TERS spectrum appears in Figure 4 alongside the calculated binding configuration that yields the simulated spectrum. The Raman spectrum is separated into these components on the basis of the expected effects of the selection rules of surface-enhanced

DOI: 10.1021/acs.jpcc.9b09162
J. Phys. Chem. C 2020, 124, 2420−2426

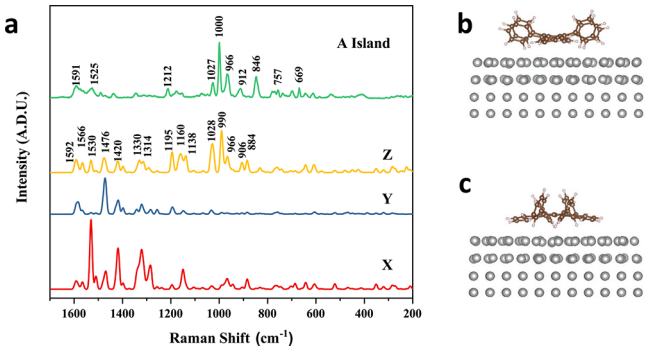

Figure 4. (a) Comparison of the experimental TERS spectrum of an A island with the simulated Raman spectrum separated into the different Cartesian coordinates. Side view of the planar binding configuration of rubrene that yielded the calculated spectrum through the (b) *y*-direction and (c) *x*-direction. The silver, brown, and white spheres represent Ag, C, and H atoms, respectively.

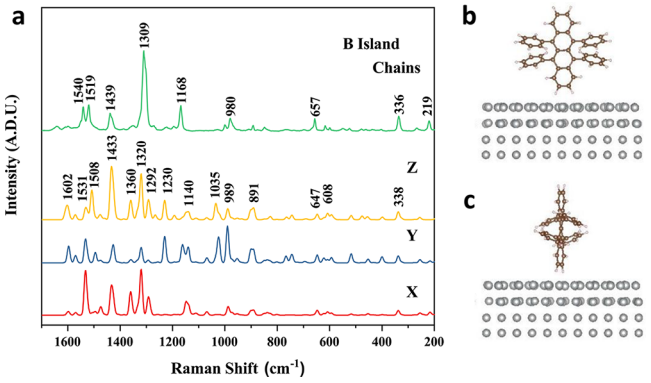

Figure 5. (a) Comparison of the experimental TERS spectrum of B islands and chains with the simulated Raman spectrum separated into the different Cartesian coordinates. Side view of the perpendicular binding configuration of rubrene that yielded the calculated spectrum through the (b) *y*-direction and (c) *x*-direction. The silver, brown, and white spheres represent Ag, C, and H atoms, respectively.

Raman spectroscopy. The vibrational modes that are perpendicular to the metal surface and parallel with the enhanced near-field are most enhanced.[55,56] This means that the *z*-component is expected to match experimental TERS spectra. The calculated vibrational modes are presented in Figure S5. The adsorption energy is 4.58 eV per rubrene molecule. Since the charge transfer between rubrene and Ag(100) is negligible, the vdW interaction is responsible for such binding. Significantly, as expected on the basis of selection rules, the *z*-component of the calculated spectrum most closely matches the experimental spectrum, reproducing the three major peaks (around 1000 cm^{-1}) of the experimental spectrum well. TERS results combined with TDDFT simulations defines the molecular binding structure in three-dimensions. Figure 4b,c describes the orientation and configuration of rubrene on the surface, revealing a slight pinch in the middle of the tetracene backbone resulting in the terminal ends tilting toward the substrate. Meanwhile, the phenyl groups are rotated about their σ bonds allowing for strong intermolecular interactions and dense packing, stabilizing the assembly, as observed on other surfaces previously by other groups.[44]

In contrast to the A islands, the rubrene molecules in B islands, chains, and even the boundaries of A islands lacked intramolecular resolution, appearing as orb-like shapes with similar vibrational fingerprints according to STM imaging and TERS. STM imaging suggests that the absence of intermolecular interactions contributes to this difference. In chains and at boundaries of A islands, the rubrene molecules interact as pairs primarily, where the opposite side of the molecule experiences minimal intermolecular interactions as it is typically bounded by bare substrate. As a result of this lack of intermolecular interaction, the rubrene molecules adopt a new orientation on the surface that has a different vibrational fingerprint compared against the planar flat orientation. Through simulations we can define this new orientation as well as the vibrational modes that result in the spectrum. These vibrational modes are depicted in Figure S6. Figure 5 presents a comparison of a representative spectrum from B islands and chains with a TDDFT determined spectrum of a rubrene molecule that adsorbs in an upright orientation. Again, the *z*-component of the simulated spectrum reproduces the major peaks of the experimental TERS results well. The adsorption energy is 2.02 eV per rubrene molecule which means that the perpendicular binding configuration is energetically less stable than the planar configuration. In this case, the perpendicular orientation is stabilized by interactions between the phenyl groups of two adjacent rubrene molecules, a similar structure and orientation that has been observed for rubrene and similar molecules on some surfaces, depending upon the strength of interactions between the molecule and the substrate.[41,57] Ultimately, the intermolecular interactions play a critical role in determining the orientation and binding configurations of rubrene on the surface.

CONCLUSION

In conclusion, the multiple configurations of rubrene on a Ag(100) surface have been characterized by STM and TERS in combination with TDDFT simulations. Our STM images show a variety of molecular superstructures: bright islands, dim islands, and chains. These various assemblies can be distinguished by the intermolecular interactions and the adsorption configurations of rubrene on the surface. The planar configuration exists within molecular islands on the surface, but at the boundaries rubrene was found to adopt a perpendicular orientation. The vibrational fingerprints obtained with TERS showed a crucial sensitivity to the binding configurations and orientations that rubrene adopts on the surface. Thus, the spatial resolution of TERS allowed the unambiguous characterization of this unique self-assembly quality. In the case of flexible polycyclic aromatic hydrocarbons, the growth of thin films and crystalline materials depends upon an understanding of the local chemical effects and intermolecular interactions that may result in amorphous character even at the smallest scales. TERS is sensitive to these highly localized factors that are critical to device fabrication through methods of bottom-up assembly.

ASSOCIATED CONTENT

Supporting Information

The Supporting Information is available free of charge on the ACS Publications website at DOI: 10.1021/acs.jpcc.9b09162.

STM image and line profiles of an A island with chains adjacent on the surface, sample experimental data with tip engaged and tip retracted TERS spectra, comparison of TERS line profile with an STM line profile, including

DOI: 10.1021/acs.jpcc.9b09162
J. Phys. Chem. C 2020, 124, 2420−2426

peak fitting and spatial resolution estimations, simulation attempts with different molecular binding configurations and orientations, models of the vibrational modes that result in the calculated vibrational spectra (PDF)

AUTHOR INFORMATION

Corresponding Author

*E-mail: njiang@uic.edu.

ORCID

Jeremy F. Schultz: 0000-0003-2231-6797

Linfei Li: 0000-0002-5217-3005

Sayantan Mahapatra: 0000-0002-7332-196X

Xu Zhang: 0000-0002-6491-3234

Nan Jiang: 0000-0002-4570-180X

Notes

The authors declare no competing financial interest.

ACKNOWLEDGMENTS

J.F.S. and N.J. acknowledge support from the National Science Foundation (CHE-1807465). C.S. and X.Z. acknowledge support from the National Science Foundation (DMR-1828019). We thank A. Undevia for his contributions in assisting with STM experiments and discussions.

REFERENCES

(1) Bartels, L. Tailoring Molecular Layers at Metal Surfaces. *Nat. Chem.* **2010**, *2* (2), 87−95.

(2) Barth, J. V. Molecular Architectonic on Metal Surfaces. *Annu. Rev. Phys. Chem.* **2007**, *58* (1), 375−407.

(3) Witte, G.; Wöll, C. Growth of Aromatic Molecules on Solid Substrates for Applications in Organic Electronics. *J. Mater. Res.* **2004**, *19* (7), 1889−1916.

(4) Hasegawa, T.; Takeya, J. Organic Field-Effect Transistors Using Single Crystals. *Sci. Technol. Adv. Mater.* **2009**, *10* (2), 024314.

(5) Jiang, N.; Kurouski, D.; Pozzi, E. A.; Chiang, N.; Hersam, M. C.; Van Duyne, R. P. Tip-Enhanced Raman Spectroscopy: From Concepts to Practical Applications. *Chem. Phys. Lett.* **2016**, *659*, 16−24.

(6) Shao, F.; Müller, V.; Zhang, Y.; Schlüter, A. D.; Zenobi, R. Nanoscale Chemical Imaging of Interfacial Monolayers by Tip-Enhanced Raman Spectroscopy. *Angew. Chem., Int. Ed.* **2017**, *56* (32), 9361−9366.

(7) Lee, J.; Tallarida, N.; Chen, X.; Liu, P.; Jensen, L.; Apkarian, V. A. Tip-Enhanced Raman Spectromicroscopy of Co(II)-Tetraphenylporphyrin on Au(111): Toward the Chemists' Microscope. *ACS Nano* **2017**, *11* (11), 11466−11474.

(8) Pozzi, E. A.; Goubert, G.; Chiang, N.; Jiang, N.; Chapman, C. T.; McAnally, M. O.; Henry, A. I.; Seideman, T.; Schatz, G. C.; Hersam, M. C.; Duyne, R. P. Ultrahigh-Vacuum Tip-Enhanced Raman Spectroscopy. *Chem. Rev.* **2017**, *117* (7), 4961−4982.

(9) Zrimsek, A. B.; Chiang, N.; Mattei, M.; Zaleski, S.; McAnally, M. O.; Chapman, C. T.; Henry, A.-I.; Schatz, G. C.; Van Duyne, R. P. Single-Molecule Chemistry with Surface- and Tip-Enhanced Raman Spectroscopy. *Chem. Rev.* **2017**, *117*, 7583.

(10) Domke, K. F.; Zhang, D.; Pettinger, B. Toward Raman Fingerprints of Single Dye Molecules at Atomically Smooth Au(111). *J. Am. Chem. Soc.* **2006**, *128* (45), 14721−14727.

(11) Domke, K. F.; Pettinger, B. In Situ Discrimination between Axially Complexed and Ligand-Free Co Porphyrin on Au(111) with Tip-Enhanced Raman Spectroscopy. *ChemPhysChem* **2009**, *10* (11), 1794−1798.

(12) Xu, X. G.; Rang, M.; Craig, I. M.; Raschke, M. B. Pushing the Sample-Size Limit of Infrared Vibrational Nanospectroscopy: From Monolayer toward Single Molecule Sensitivity. *J. Phys. Chem. Lett.* **2012**, *3* (13), 1836−1841.

(13) Mahapatra, S.; Ning, Y.; Schultz, J. F.; Li, L.; Zhang, J.-L.; Jiang, N. Angstrom Scale Chemical Analysis of Metal Supported Trans- and Cis-Regioisomers by Ultrahigh Vacuum Tip-Enhanced Raman Mapping. *Nano Lett.* **2019**, *19* (5), 3267−3272.

(14) Witlicki, E. H.; Hansen, S. W.; Christensen, M.; Hansen, T. S.; Nygaard, S. D.; Jeppesen, J. O.; Wong, E. W.; Jensen, L.; Flood, A. H. Determination of Binding Strengths of a Host−Guest Complex Using Resonance Raman Scattering. *J. Phys. Chem. A* **2009**, *113* (34), 9450−9457.

(15) Nelson, D. A.; Schultz, Z. D. Influence of Optically Rectified Electric Fields on the Plasmonic Photocatalysis of 4-Nitrothiophenol and 4-Aminothiophenol to 4,4-Dimercaptoazobenzene. *J. Phys. Chem. C* **2018**, *122* (15), 8581−8588.

(16) Chiang, N.; Jiang, N.; Madison, L. R.; Pozzi, E. A.; Wasielewski, M. R.; Ratner, M. A.; Hersam, M. C.; Seideman, T.; Schatz, G. C.; Van Duyne, R. P. Probing Intermolecular Vibrational Symmetry Breaking in Self-Assembled Monolayers with Ultrahigh Vacuum Tip-Enhanced Raman Spectroscopy. *J. Am. Chem. Soc.* **2017**, *139* (51), 18664−18669.

(17) Whiteman, P. J.; Schultz, J. F.; Porach, Z. D.; Chen, H.; Jiang, N. Dual Binding Configurations of Subphthalocyanine on Ag(100) Substrate Characterized by Scanning Tunneling Microscopy, Tip-Enhanced Raman Spectroscopy, and Density Functional Theory. *J. Phys. Chem. C* **2018**, *122* (10), 5489−5495.

(18) Zhang, Y.; Zhang, R.; Jiang, S.; Zhang, Y.; Dong, Z.-C. Probing Adsorption Configurations of Small Molecules on Surfaces by Single-Molecule Tip-Enhanced Raman Spectroscopy. *ChemPhysChem* **2019**, *20*, 37.

(19) Jiang, N.; Chiang, N.; Madison, L. R.; Pozzi, E. A.; Wasielewski, M. R.; Seideman, T.; Ratner, M. A.; Hersam, M. C.; Schatz, G. C.; Van Duyne, R. P. Nanoscale Chemical Imaging of a Dynamic Molecular Phase Boundary with Ultrahigh Vacuum Tip-Enhanced Raman Spectroscopy. *Nano Lett.* **2016**, *16* (6), 3898−904.

(20) Chiang, N.; Chen, X.; Goubert, G.; Chulhai, D. V.; Chen, X.; Pozzi, E. A.; Jiang, N.; Hersam, M. C.; Seideman, T.; Jensen, L.; Van Duyne, R. P. Conformational Contrast of Surface-Mediated Molecular Switches Yields Angstrom-Scale Spatial Resolution in Ultrahigh Vacuum Tip-Enhanced Raman Spectroscopy. *Nano Lett.* **2016**, *16* (12), 7774−7778.

(21) Liu, P.; Chen, X.; Ye, H.; Jensen, L. Resolving Molecular Structures with High-Resolution Tip-Enhanced Raman Scattering Images. *ACS Nano* **2019**, *13* (8), 9342−9351.

(22) Li, Z.; Du, J.; Tang, Q.; Wang, F.; Xu, J.-B.; Yu, J. C.; Miao, Q. Induced Crystallization of Rubrene in Thin-Film Transistors. *Adv. Mater.* **2010**, *22* (30), 3242−3246.

(23) Sutton, C.; Marshall, M. S.; Sherrill, C. D.; Risko, C.; Brédas, J.-L. Rubrene: The Interplay between Intramolecular and Intermolecular Interactions Determines the Planarization of Its Tetracene Core in the Solid State. *J. Am. Chem. Soc.* **2015**, *137* (27), 8775−8782.

(24) Campione, M. Rubrene Heteroepitaxial Nanostructures With Unique Orientation. *J. Phys. Chem. C* **2008**, *112* (42), 16178−16181.

(25) Nečas, D.; Klapetek, P. Gwyddion: An Open-Source Software for SPM Data Analysis. *Cent. Eur. J. Phys.* **2012**, *10* (1), 181−188.

(26) Kresse, G.; Furthmüller, J. Efficient Iterative Schemes for Ab Initio Total-Energy Calculations Using a Plane-Wave Basis Set. *Phys. Rev. B: Condens. Matter Mater. Phys.* **1996**, *54* (16), 11169−11186.

(27) Blöchl, P. E. Projector Augmented-Wave Method. *Phys. Rev. B: Condens. Matter Mater. Phys.* **1994**, *50* (24), 17953−17979.

(28) Perdew, J. P.; Burke, K.; Ernzerhof, M. Generalized Gradient Approximation Made Simple. *Phys. Rev. Lett.* **1996**, *77* (18), 3865−3868.

(29) Grimme, S. Semiempirical GGA-Type Density Functional Constructed with a Long-Range Dispersion Correction. *J. Comput. Chem.* **2006**, *27* (15), 1787−1799.

(30) Baroni, S.; de Gironcoli, S.; Dal Corso, A.; Giannozzi, P. Phonons and Related Crystal Properties from Density-Functional Perturbation Theory. *Rev. Mod. Phys.* **2001**, *73* (2), 515−562.

DOI: 10.1021/acs.jpcc.9b09162
J. Phys. Chem. C 2020, 124, 2420−2426

(31) Zhang, X. Large-Scale Ab Initio Calculations of Raman Scattering Spectra within Time-Dependent Density Functional Perturbation Theory. *J. Chem. Phys.* **2018**, *148* (24), 244103.
(32) Ma, L.; Zhang, K.; Kloc, C.; Sun, H.; Michel-Beyerle, M. E.; Gurzadyan, G. G. Singlet Fission in Rubrene Single Crystal: Direct Observation by Femtosecond Pump−Probe Spectroscopy. *Phys. Chem. Chem. Phys.* **2012**, *14* (23), 8307−8312.
(33) Haes, A. J.; Zou, S.; Zhao, J.; Schatz, G. C.; Van Duyne, R. P. Localized Surface Plasmon Resonance Spectroscopy near Molecular Resonances. *J. Am. Chem. Soc.* **2006**, *128* (33), 10905−10914.
(34) Zhao, J.; Jensen, L.; Sung, J.; Zou, S.; Schatz, G. C.; Van Duyne, R. P. Interaction of Plasmon and Molecular Resonances for Rhodamine 6G Adsorbed on Silver Nanoparticles. *J. Am. Chem. Soc.* **2007**, *129* (24), 7647−7656.
(35) Pivetta, M.; Blüm, M.-C.; Patthey, F.; Schneider, W.-D. Coverage-Dependent Self-Assembly of Rubrene Molecules on Noble Metal Surfaces Observed by Scanning Tunneling Microscopy. *ChemPhysChem* **2010**, *11* (7), 1558−1569.
(36) Blüm, M.-C.; Ćavar, E.; Pivetta, M.; Patthey, F.; Schneider, W.-D. Conservation of Chirality in a Hierarchical Supramolecular Self-Assembled Structure with Pentagonal Symmetry. *Angew. Chem., Int. Ed.* **2005**, *44* (33), 5334−5337.
(37) Viereck, J.; Rangan, S.; Häberle, P.; Galoppini, E.; Douglas, C. J.; Bartynski, R. A. Rubrene Versus Fluorine-Functionalized Rubrene Molecules on a Metal Surface: Self-Assembly, Electronic Structure, and Energy Alignment of a Monolayer on Ag(100). *J. Phys. Chem. C* **2019**, *123*, 14382.
(38) Käfer, D.; Ruppel, L.; Witte, G.; Wöll, C. Role of Molecular Conformations in Rubrene Thin Film Growth. *Phys. Rev. Lett.* **2005**, *95* (16), 166602.
(39) He, Y.; Bussolotti, F.; Xin, Q.; Yang, J.; Kera, S.; Ueno, N.; Duhm, S. Transient Monolayer Structure of Rubrene on Graphite: Impact on Hole−Phonon Coupling. *J. Phys. Chem. C* **2016**, *120* (27), 14568−14574.
(40) Duhm, S.; Xin, Q.; Hosoumi, S.; Fukagawa, H.; Sato, K.; Ueno, N.; Kera, S. Charge Reorganization Energy and Small Polaron Binding Energy of Rubrene Thin Films by Ultraviolet Photoelectron Spectroscopy. *Adv. Mater.* **2012**, *24* (7), 901−905.
(41) Wang, J.-Z.; Lan, M.; Shao, T.-N.; Li, G.-Q.; Zhang, Y.; Huang, C.-Z.; Xiong, Z.-H.; Ma, X.-C.; Jia, J.-F.; Xue, Q.-K. STM Study of a Rubrene Monolayer on Bi(001): Structural Modulations. *Phys. Rev. B: Condens. Matter Mater. Phys.* **2011**, *83* (23), 235433.
(42) Pivetta, M.; Blüm, M.-C.; Patthey, F.; Schneider, W.-D. Two-Dimensional Tiling by Rubrene Molecules Self-Assembled in Supramolecular Pentagons, Hexagons, and Heptagons on a Au(111) Surface. *Angew. Chem., Int. Ed.* **2008**, *47* (6), 1076−1079.
(43) Pivetta, M.; Blüm, M.-C.; Patthey, F.; Schneider, W.-D. Three-Dimensional Chirality Transfer in Rubrene Multilayer islands on Au(111). *J. Phys. Chem. B* **2009**, *113* (14), 4578−4581.
(44) Wang, L.; Kong, H.; Chen, X.; Du, X.; Chen, F.; Liu, X.; Wang, H. Conformation-Induced Self-Assembly of Rubrene on Au(111) Surface. *Appl. Phys. Lett.* **2009**, *95* (9), 093102.
(45) Jarvis, S. P. Resolving Intra- and Inter-Molecular Structure with Non-Contact Atomic Force Microscopy. *Int. J. Mol. Sci.* **2015**, *16* (8), 19936−19959.
(46) Gross, L.; Mohn, F.; Moll, N.; Liljeroth, P.; Meyer, G. The Chemical Structure of a Molecule Resolved by Atomic Force Microscopy. *Science* **2009**, *325* (5944), 1110−1114.
(47) Chen, C. J. *Introduction to Scanning Tunneling Microscopy*; Oxford University Press USA - OSO: Cary, NC, 1993.
(48) Mukherjee, T.; Sinha, S.; Mukherjee, M. Electronic Structure of Twisted and Planar Rubrene Molecules: a Density Functional Study. *Phys. Chem. Chem. Phys.* **2018**, *20* (27), 18623−18629.
(49) Stöckle, R. M.; Suh, Y. D.; Deckert, V.; Zenobi, R. Nanoscale Chemical Analysis by Tip-Enhanced Raman Spectroscopy. *Chem. Phys. Lett.* **2000**, *318* (1−3), 131−136.
(50) Hayazawa, N.; Inouye, Y.; Sekkat, Z.; Kawata, S. Metallized Tip Amplification of Near-Field Raman Scattering. *Opt. Commun.* **2000**, *183* (1−4), 333−336.
(51) Anderson, M. S. Locally Enhanced Raman Spectroscopy with an Atomic Force Microscope. *Appl. Phys. Lett.* **2000**, *76* (21), 3130−3132.
(52) Zhang, R.; Zhang, Y.; Dong, Z. C.; Jiang, S.; Zhang, C.; Chen, L. G.; Zhang, L.; Liao, Y.; Aizpurua, J.; Luo, Y.; Yang, J. L.; Hou, J. G. Chemical Mapping of a Single Molecule by Plasmon-Enhanced Raman Scattering. *Nature* **2013**, *498* (7452), 82−6.
(53) Lee, J.; Crampton, K. T.; Tallarida, N.; Apkarian, V. A. Visualizing Vibrational Normal Modes of a Single Molecule with Atomically Confined Light. *Nature* **2019**, *568* (7750), 78−82.
(54) Mahapatra, S.; Schultz, J. F.; Ning, Y.; Zhang, J.-L.; Jiang, N. Probing Surface Mediated Configurations of Nonplanar Regioisomeric Adsorbates using Ultrahigh Vacuum Tip-Enhanced Raman Spectroscopy. *Nanoscale* **2019**, *11*, 19877−19833.
(55) Moskovits, M.; Suh, J. S. Surface Selection Rules for Surface-Enhanced Raman Spectroscopy: Calculations and Application to the Surface-Enhanced Raman Spectrum of Phthalazine on Silver. *J. Phys. Chem.* **1984**, *88* (23), 5526−5530.
(56) Gao, X.; Davies, J. P.; Weaver, M. J. Test of Surface Selection Rules for Surface-Enhanced Raman Scattering: the Orientation of Adsorbed Benzene and Monosubstituted Benzenes on Gold. *J. Phys. Chem.* **1990**, *94* (17), 6858−6864.
(57) Briseno, A. L.; Aizenberg, J.; Han, Y.-J.; Penkala, R. A.; Moon, H.; Lovinger, A. J.; Kloc, C.; Bao, Z. Patterned Growth of Large Oriented Organic Semiconductor Single Crystals on Self-Assembled Monolayer Templates. *J. Am. Chem. Soc.* **2005**, *127* (35), 12164−12165.

DOI: 10.1021/acs.jpcc.9b09162
J. Phys. Chem. C 2020, 124, 2420−2426